Silicon Photoanodes for Solar-Driven Oxidation of Brine: A Nanoscale, Photo-Active Analog of the Dimensionally-Stable Anode

Silicon Photoanodes for Solar-Driven Oxidation of Brine: A Nanoscale, Photo-Active Analog of the Dimensionally-Stable Anode

Robert Tang-Kong[a,†], Christopher O'Rourke[b,†], Andrew Mills[b], and Paul C. McIntyre[a]*

a: Department of Materials Science & Engineering, Stanford University, California 94305, USA

b: Department of Chemistry and Chemical Engineering, Queens University Belfast, Stranmillis Road, Belfast, BT9 5AG, UK

† These authors contributed equally to this work

* e-mail: pcm1@stanford.edu

Abstract

We report the first results in which ALD-TiO_2 layers electronically couple silicon to an overlying catalyst coating while inhibiting corrosion during brine splitting, a reaction that is capable of generating not only a fuel (H_2) but also a disinfectant (Cl_2 or NaOCl). An n-type silicon photoanode, and a p+-silicon anode are protected by a 1.7 nm coating of amorphous TiO_2 and 2 nm coating of Ir. The p+-Si/TiO_2/Ir anode is able to effect the oxidation of chloride (0.5 M H_2SO_4, 3.5 M NaCl) in the dark with a low overpotential compared to that for oxidation of water (0.5 M H_2SO_4). The 0.294 V overpotential difference occurs despite the difference in standard redox potentials, $\Delta E = (E^o(Cl_2/Cl^-) - E^o(O_2/H_2O))$, is 130 mV. Under 1 sun irradiation a photovoltage of *ca.* 0.566 V is achieved by comparing the illuminated n-Si/TiO_2/Ir photoanode with the dark p+-silicon anode. Although the n-Si/TiO_2/Ir photoanode is only one half of an eventual tandem cell needed for photosynthetic brine splitting, its ABPE for chloride oxidation is 1.42%, *ca.* 28 times that for water oxidation. The illuminated n-Si/TiO_2/Ir photoanode remained stable at 1 mA cm^{-2} during a six-day chronopotentiometry test.

Key words: silicon; anode; brine; chloride; oxidation; photoelectrochemistry

I. Introduction

Conversion of solar to electrical energy using photovoltaic devices, such as the silicon solar cell is well-established, but solar energy is diurnal and intermittent and so there is least of it when we most need it, i.e. at night in winter. As a consequence, there is great interest in developing efficient, inexpensive and stable solar energy conversion devices that generate readily utilizable chemical fuels.[1,2] A popular, current approach is to develop a solar-driven, water-splitting system, since it uses the sun's energy to produce hydrogen, which can be stored, readily transported and used when needed.[2] However, the overpotential for water oxidation, using the best platinum group metal electrocatalysts[1], is still typically 300-400 mV at 10 mA cm^{-2} and so represents a major barrier to the creation of a long-lasting, high solar to chemical energy efficiency device.

Recently, Nocera et al. suggested that an inexpensive artificial leaf water splitting device will find initial and widespread application in the developing world at less urbanized, off-the-grid, locations.[3,4] Advantages of such photoelectrochemical cells (PEC's) which combine light absorption and catalyzed electrochemical reactions are 1) the potential simplicity of an integrated design, 2) their compact foot-print and 3) their ability to accommodate less expensive catalysts operating at electrolysis current densities better matched to solar photocurrent densities.

Compared to the photocleavage of water, the photo-electrolysis of brine has not been studied nearly as widely, despite the fact that the overpotential for chlorine production is low.[5] In addition, the electrolysis of salt water: (i) generates H_2, alkali and Cl_2, (or, H_2 and NaOCl, if the Cl_2 and caustic are allowed to combine), (ii) stores approximately the same amount of energy per electron as the water splitting reaction, and (iii) generates a more valuable chemical oxidant feedstock, namely, Cl_2 or NaOCl. However, it is not without its challenges, given the oxidation of chloride to chlorine in acid solution

$$2Cl^- \rightleftharpoons 2Cl_2 + 2e^- \quad (1)$$

has a significantly higher standard redox potential ($E^o(Cl_2/Cl^-)$ = 1.36 V) than that of water

$$H_2O \rightleftharpoons 2H^+ + \tfrac{1}{2}O_2 + 2e^- \quad (2)$$

($E^o(O_2/H_2O)$ = 1.23 V). Moreover, chlorine is a very aggressive oxidant, with a solubility in water (0.092 mol dm^{-3} atm^{-1}) that is over 70 x's that of O_2, thus increasing markedly the likelihood of its reaction with cell components, including, most importantly, the semiconductor photoanode.

The industrial production of Cl_2/NaOCl from brine is worth currently $46 Bn in the USA alone.[6] Its role in disinfection is important, since the need for potable (i.e. disinfected) water worldwide is great, with a sixth of the world population (ca. 1.1 Bn people) having no access to improved water supplies and with a much greater number consuming contaminated water every day. It is estimated that > 4000 children die of diarrhoea alone every day due to poor water quality.[7] There is, therefore, a compelling need for an inexpensive and compact solar-to-chemical energy conversion device capable of producing not only a fuel (hydrogen), for heating and for electricity (via a fuel cell), when the sun is not shining, but also a disinfectant – such as chlorine/hypochlorite – for use in generating potable water and clean surfaces.

Herein we report a silicon photoanode which functions both as a nanoscale version of the dimensionally-stable anode (DSA)[8], the key technology in industrial chlor-alkali electrochemistry, and as an efficient absorber of solar light. This photoanode could function as a key junction in a multi-junction photoelectrochemical cell[9] for unassisted brine splitting. Industrial DSA electrodes have a high precious metal (Ir, Ru) loading and thick active layers[10] mixed with TiO_2 and typically coating a Ti substrate.[11,12] However, such anodes typically operate at current densities that are 100 x's greater than those (ca. 10 mA cm^{-2}) expected in any photosynthetic solar cell and In the reported nanoscale DSA structure, atomic layer deposited TiO_2 is used to achieve stable brine splitting on silicon, which is otherwise unstable under the conditions used in chloride oxidation. The TiO_2 thin film electronically couples an overlying chloride oxidation catalyst film, in the form of an ultra-thin iridium layer, to the silicon substrate, achieving a high yield for chlorine synthesis, photovoltages exceeding 560 mV and greater than 6 days of continuous operation during chronoamperometry testing.

II. Experimental

Materials

The silicon wafers used here were either: (i) heavily boron-doped p^+-type Si (100) wafers (ρ = 0.001–0.002 Ω cm, 500 μm thick), which were used as conductive silicon substrates to study water and chloride oxidation in the dark or (ii) lightly phosphorous-doped, n-type Si (100) wafers (ρ = 0.1–0.2 Ω cm, 500 μm thick). The wafers were used as received, with a thin (< 2 nm) SiO_2 layer as prepared by the wafer supplier, Nova Electronic Materials. Onto both wafer types, a 1.7 nm amorphous TiO_2 layer was deposited via 30 cycles of atomic layer deposition, ALD, at 170ºC with tetrakis-dimethylamido titanium, TDMAT, as the titanium source and H_2O as the oxygen source. In all cases, this was followed by a coating of a 2 nm Ir layer, deposited by electron beam evaporation. The backside contacts for the n-Si and p^+-Si substrates were e-beam evaporated Al and Pt, respectively. These two electrodes are referred to throughout as n-Si/TiO_2/Ir and p+-Si/TiO_2/Ir electrodes. A schematic of the n-Si/TiO_2/Ir photoanode used in this work for the photoelectrolysis of acidified brine is illustrated in **Figure 1**.

Methods

All electrochemical and photoelectrochemical experiments were conducted using 0.5 mol dm^{-3} H_2SO_4, in the absence (for water oxidation) and presence (for chloride oxidation) of 3.5 mol dm^{-3} NaCl. All electrochemical work was performed using a modified version of the 'silo-like' electrochemical cell used by the McIntyre and Chidsey group,[13] which is illustrated in **Figure S1**. The cell components and design are described in the supporting information. The gas inlet and outlet of the cell were used in Cl_2 yield measurements to sweep out, using a continuous stream of Ar (flow rate: 100 cm^3 min^{-1}), the Cl_2 generated in the electrochemical cell into a 100 cm^3 KI trap the spectrophotometric analysis of the latter allowed the total amount of Cl_2 to be assessed [14]. The bulk of the electrochemical measurements were conducted using a Metrohm Autolab (PGSTAT128N) potentiostat. All linear sweep voltammograms, LSVs, were recorded using a 1 mV s^{-1} sweep rate. Electrochemical impedance spectroscopy was performed using a FRA32M module (Metrohm) in order to determine the resistance of electrolytes used in this study and so compensate for the *i*R drop in the cell.

A sealed, quartz window recessed in the PTFE cap of the electrochemical cell allowed the flat, n-Si/TiO_2/Ir anode, installed in the base of the cell, to be irradiated. Irradiations were conducted using either: (i) a high power 455 nm LED (HBW = 16 nm; OSLON+ PowerStar Deep Blue 455 nm; maximum wattage > 2.2 W) providing an irradiance of ca. 6.5 mW cm^{-2} (at ca. 7 cm above the electrode) for the chronopotentiometry experiments or, more usually, (ii) a 150 W solar simulator (Sciencetech SS150W) fitted with a AM1.5 filter, simulating the irradiance of 1 sun (ca. 100 mW cm^{-2}, measured using a power meter, ThorLabs, PM100D). All UV/Vis spectra were recorded using an Agilent Cary 6000i UV/Vis/NIR spectrophotometer. IPCE measurements were made using a standard glass vial (A-001056, Biologic) with a PTFE cap holding all electrodes in place and a1kW Xe-arc lamp (OBB KiloArc), coupled to a 200 mm meter Czerny-Turner monochromator (OBB), and Gooch & Housego (OL756) radiometer were used to provide the monochromatic light and associated irradiance values, respectively. IPCE measurements were conducted on a n-Si/TiO_2/Ir photoanode (area: 0.8 cm^2) polarised at 1.8 v vs NHE in an electrolyte volume of 15mL (0.5M H_2SO_4 + 3.5 NaCl).

III. Results and Discussion

Optical measurements and initial photoelectrochemical studies

Silicon, a candidate material for the low-gap semiconductor of a tandem device, has a band gap of 1.1 eV and so absorbs strongly incident light of $\lambda \leq 1127$ nm, as indicated by its reflectance spectrum which has been widely reported.[15]

In contrast to the absorption spectrum of Si, those of the protecting Ti oxide and the Ir film used in this work have not been reported previously. Thus, the UV/Vis/NIR absorption spectrum of the thin (1.7 nm) TiO_2 film, deposited using ALD on quartz, is illustrated in **Figure 2**and shows that it absorbs no visible light, i.e. it is colourless, and that it absorbs very little UV radiation. Thus, its presence will have very little effect on the amount of light absorbed by the underlying Si. In contrast, the absorption spectrum of the 2 nm Ir film, also illustrated in **Figure 2**, reveals an average absorbance of ca. 0.184 throughout the visible and NIR spectrum, which suggests that only ca. 65.5 % of the incident visible light is transmitted by the Ir film to the underlying Si. Thus, although the deposition

of an Ir film is convenient and relatively easy to effect, the use of the Ir catalyst in the form of a continuous film reduces the efficiency of the photoanode significantly by partly obscuring the surface of the Si. This implies that the photocurrent may be improved markedly if a pattern of catalyst islands is used instead of a film. This approach has been adopted in the work of Hu et al[16] who used 100 nm thick Ni-island electrocatalysts patterned in square arrays of 3 μm diameter circles on a 7-μm pitch, to cover thick (44 nm), but 'electronically leaky', TiO_2 protective coatings on an n-Si photoanode film, so that the islands only blocked 14.4% of the electrode surface.

In order to quickly compare and contrast the efficacies of the n-Si/TiO_2/Ir photoanode for water oxidation (in 0.5 M H_2SO_4) to that of chloride (in 0.5 M H_2SO_4 plus 3.5 M NaCl), cyclic voltammograms photocurrents were recorded under 1 sun irradiation and the results of this work are illustrated in **Figure 4**.

Inspection of the results reveals that n-Si/TiO_2/Ir photoanode is able to effect the photo-oxidation of chloride to chlorine in acid at lower potentials (typically, ca. 300 mV lower at 1 mA cm^{-2}) than that for water oxidation, despite the fact that $\Delta E = (E^o(Cl_2/Cl^-) - E^o(O_2/H_2O)) = 130$ mV. This feature results from the much higher overpotential for water oxidation, η_{O2}, ($\eta_{O2} \approx 0.428$ V on a p+-Si/TiO_2/Ir anode, vide infra) compared to that for chloride oxidation ($\eta_{Cl2} \approx$ ca. 0.134 V on a p+-Si/TiO_2/Ir anode, vide infra).

In contrast, in 1 M NaOH, the primary chloride oxidation reaction is:

$$Cl^- + 2OH^- \rightleftharpoons OCl^- + 2H_2O + 2e^- \quad (3)$$

where, ($E^o(OCl^-/Cl^-) = 0.81$ V vs NHE, so that ΔE, now equal to: ($E^o(OCl^-/Cl^-) - E^o(O_2/OH^-)$, is much larger (406 mV), than the 130 mV in acid, and this mostly off-sets the benefit gained by having $\eta_{Cl2} << \eta_{O2}$. Thus, in 1 M NaOH the CV curves for water and chloride oxidation are no longer well separated, but overlap, so that the photoanode generates a mixture of hypochlorite and O_2. As a consequence, in order to simplify this study to that of either water or chloride oxidation, but not a mixture of both, the bulk of the work described here was carried out under acidic conditions (0.5 M H_2SO_4) with or without 3 M NaCl. In acidified brine the overall photo-electrochemical reaction is the

oxidation of chloride to Cl_2, i.e. reaction (1), at the n-Si/TiO_2/Ir photoanode, and the concomitant reduction of H^+ to H_2 at the Pt counter electrode, as illustrated in **Figure 1**.

It can be shown[13] that solar irradiation at 1 sun provides ca. $2.7x10^{17}$ photons cm^{-2} with energies ≥ the Si band gap, which in turn should produce a theoretical maximum photocurrent density of ca. 43 mA cm^{-2}. From the results illustrated in **Figure 4**, the light-limited saturation currents for both water and chloride oxidation, achieved at high bias potentials, were found to be ca. 31 mA cm^{-2}, i.e. ca. 72% of the theoretical maximum. Given that ca. 35% of the incident light is obscured by the Ir film, the value of 72% implies that, at high bias potentials, the n-Si/TiO_2/Ir photoanode, is ca. 100% efficient in converting photons to current, i.e. the photogenerated holes are readily and efficiently conducted through the TiO_2 overlayer to the Ir electrocatalyst. IPCE measurements were also made using the n-Si/TiO_2/Ir photoanode biased at 1.8V vs NHE (Figure **4**). The IPCE is high, across a wide range of wavelengths, and consistent with the average value of 72% reported above, suggesting that, once corrected for the absorbance due to the catalyst layers, this system, with its 1.8 V bias is ca. 100% efficient in converting photons to current.

The broken vertical lines in **Figure 4** represent the thermodynamic redox potentials for water (black) and chloride (red) oxidation in 0.5 M H_2SO_4 and in both photo-electrochemical reactions, reasonable (up to 10 mA cm^{-2} and 1 mA cm^{-2} for Cl^- and H_2O oxidation, respectively) photocurrents are generated, by the n-Si/TiO_2/Ir photoanode at 1 sun illumination, at potentials at and below these thermodynamic limits, suggesting a reasonable degree of solar to chemical energy conversion, although clearly much more so for chloride oxidation. However, as we shall see later, a useful assessment of the applied bias photon efficiency, ABPE, requires the cell to be operated in 2-electrode, rather than 3-electrode mode, and under such conditions the efficiency of cell is significantly reduced.

The above results show that, upon band gap illumination of the n-Si, the photogenerated holes in the Si valence band are able to move through the intermediate oxide layers, as illustrated in **Figure 1**, to the Ir layer, where they are then able to oxidize surface adsorbed water, or chloride, from the electrolyte solution. Further work on TiO_2-protected Si anodes,[19–22] suggests that the unexpectedly

low barrier for hole conduction through the amorphous TiO_2 layer involves hole-tunnelling through an ultrathin (< 2 nm) SiO_2 interface layer and then a polaronic or hopping conduction mechanism through the TiO_2 protective layer to the Ir catalyst film. Importantly, in the absence of light, the current is negligible, i.e. < 1 μA cm^{-2}, at the potentials used in **Figure 4**, due to the very low thermal population of holes in the n-Si. Thus, in the dark the n-Si/TiO_2/Ir photoanode is not able to effect either the water oxidation or chloride oxidation half-cell reactions, but is able to do so upon illumination with ultra-band gap light, as illustrated by the photoelectrochemical data in **Figure 4**.

LSV's: Tafel slopes, overpotentials and photovoltages

Linear sweep voltammograms, LSVs, for water oxidation, i.e. reaction (2), were recorded for the n-Si/TiO_2/Ir photoanode, under 1 sun illumination, and the p+-Si/TiO_2/Ir anode (in the dark) in 0.5 M H_2SO_4 and the results are illustrated in **Figure 5**(a). Similarly, LSVs for *chloride oxidation*, i.e. reaction (1), were recorded for the n-Si/TiO_2/Ir photoanode – under 1 sun illumination, and the p+-Si/TiO_2/Ir anode (in the dark) in a (0.5 M H_2SO_4 plus 3.5 M NaCl) electrolyte and the results are illustrated in **Figure 5**(b). The broken vertical lines highlight the formal redox potentials, $E^{o'}$, of the O_2/H_2O (black) and Cl^-/Cl_2 (red) couples in 0.5 M H_2SO_4 and (0.5 M H_2SO_4 plus 3.5 M NaCl) electrolytes, respectively, calculated, using the Nernst equation, to be: 1.212 and 1.328 V, respectively.

The data associated with each of the LSV's illustrated in **Figure 5** provides a good fit to the Tafel equation, i.e. [23]

$$\eta = a + b \bullet \log(i) \qquad (4)$$

where, η = overpotential (= applied bias, V_b, - $E^{o'}$), *a* and *b* are constants (units: V) and *i* is the current density (units: mA cm^{-2}). It follows from eqn (4) that the value of the constant '*a*' is the overpotential necessary to generate a current/photocurrent density of 1 mA cm^{-2} and '*b*' is the Tafel slope, which can provide an insight into the mechanism that underpins the associated electrochemical oxidation. A summary of the *a* and *b* terms determined by this analysis for the two electrodes in the two different electrolytic solutions, derived from Tafel plots of the data in **Figure 5**, is given in **Table 1**. The '*a'*

values in parenthesis for water oxidation are those reported by Chen et al. [13] for similar electrodes, although with a thicker Ir layer, i.e. 3 nm rather than the 2 nm used here, and in 1 M H_2SO_4. Reassuringly both studies report a very similar photovoltage, i.e. 0.568 V compared with the value of 0.532 V reported by Chen et al.[13]. As noted by these workers, this photovoltage is similar to that of the best Si photoelectrochemical solar cells.[24]

Table 1 shows the Tafel slope to be between 70-80mV/decade, with previous works reporting Tafel slopes in the range of 34-54mV/decade[5,25,26] for iridium oxide catalysts. Slopes around 40mV/decade are commonly attributed to a Heyrovsky-type rate limiting step,[27] and are associated with electrochemical desorption being slow.[5] It is worth noting that these previous works study iridium oxide materials, synthesized either by electrochemical cycling or thermal decomposition[25]. This work employs an iridium metal catalyst that may not fully oxidize during operation, which may result in different Tafel slopes for those more reduced regions. This is in agreement with Tilak's work, which subjected iridium anodes to cathodic current prior to testing and saw higher Tafel slopes (46-54mV/decade) for a more reduced iridium catalyst.[5] Despite these slightly sub-optimal Tafel slopes, these ALD-TiO_2 protection layers have been shown to support a wide variety of catalyst materials for the water oxidation reaction[19,28], implying the protection layer is robust enough to support further optimization of the catalyst layer.

Cl_2 yield and stability

As note earlier, examination of either the CV data in **Figure 4**, or the LSV data in **Figure 5**, reveals a significant separation (i.e. ca. 0.290 V from data in **Table 1**) between the two photocurrent LSV plots for the n-Si/TiO_2/Ir, under 1 sun illumination, in the two different electrolytes, 0.5 M H_2SO_4 and (0.5 M H_2SO_4 + 3.5 M NaCl), respectively. A similar separation is found for the p+-Si/TiO_2/Ir anode (i.e. 0.294 V from data in **Table 1**). This feature suggests that when operated at a modest photocurrent, or current, (i.e. 1-2 mA) the n-Si/TiO_2/Ir photoanode, or p+-Si/TiO_2/Ir anode, should, almost exclusively, mediate the oxidation of chloride, reaction (1), rather than that of water, reaction (2), so that the yield

238 of chlorine should be very high. In order to test this prediction, the Si/TiO_2/Ir photoanode (under 1
239 sun irradiation, polarized at 0.72 V vs Ag/AgCl) and the p+-Si/TiO_2/Ir anode (in dark, polarized at
240 1.18 V vs Ag/AgCl) were operated in chronoamperometric mode for 1 hour, during which not only
241 was the current monitored but also any chlorine generated in the electrochemical cell was swept, by a
242 continual stream of Ar, from the electrolyte to an aqueous trap solution (100 cm^3), comprising a
243 mixture of KI (0.36 M), NaOH (0.025 M) and potassium hydrogen phthalate (0.049 M)[29]. Previous
244 work has demonstrated that the latter solution acts as a very efficient trap for chlorine in a stream of
245 an inert gas, but not for oxygen. In the trap the Cl_2 reacts with the iodide in the trap solution to form
246 tri-iodide, the concentration of which can then be assessed spectrophotometrically, given the molar
247 absorptivity $\varepsilon(I_3^-)$ = 26400 L cm^{-1} mol^{-1} at 353 nm.[14]

248 **Figure 6** illustrates the chronoamperograms recorded for the Si/TiO_2/Ir photoanode and the p+-
249 Si/TiO_2/Ir anode in an electrolyte of (0.5 M H_2SO_4 + 3.5 M NaCl). The initial drift downwards in
250 current does not appear to be due to the loss of electrocatalyst as the same feature was observed in a
251 repeat experiment using the same, used, electrodes and was also observed when an Ir rod was used as
252 the anode. Instead, it appears to be due to gas bubble formation on the surface of the electrodes.
253 From the ratio of the total amount of triodide trapped (3.13 x 10^{-6} moles for the n-Si/TiO_2/Ir
254 photoanode) to the total amount of charge passed (Q = 0.71 C for the n-Si/TiO_2/Ir photoanode)
255 Faradaic efficiencies for Cl_2 production were determined to be 85% and 92% for the nSi/TiO_2/Ir
256 photoanode and the p+-Si/TiO_2/Ir anode, respectively. Similar yields were determined using an Ir rod
257 as the anode and also a dimensionally stable anode, comprising a film of RuO_2/TiO_2 on a Ti foil [30],
258 and the slightly less than 100% Faradaic efficiencies for Cl_2 production for all these electrodes was
259 attributed to a small degree of reaction of the very aggressively oxidising chlorine with the
260 components of the system as it was swept from the electrochemical cell to the trap solution.

261 Chlorine is a very reactive oxidising agent, thus any protective coating has to be sufficiently robust
262 *chemically* to withstand the highly corrosive action of chlorine in a highly acidic environment.
263 Without this TiO_2 coating, even with an Ir catalyst layer, none of the p+-Si and n-Si anodes are stable
264 and able to effect the oxidation of either water or chloride. In order to probe the stability of the TiO_2

protective coating and the overall photostability of the photonaode, a chronopotentiogram was recorded, with the current set at 1 mA cm^{-2}, for the Si/TiO_2/Ir photoanode (irradiated with a UV 455 nm LED; 6.5 mW cm^{-2}) over a period of ca 6 days and the results are illustrated in **Figure 7**.

The short disruption in the current –time plot at 3 d, see **Figure 7**, was due to Cl_2 bubble formation, which – once cleared – allowed the photoelectrode to function as before. The %Cl_2 yield was measured for the first and last hour of this run and found to be in both cases ca. 85% as in **Figure 6**. The results illustrated in **Figure 7** indicate that the n-Si/TiO_2/Ir photoanode is stable over a 6-day period when used to photo-electrochemically oxidized chloride to chlorine under acidic conditions.

Films as-deposited are conformal, metallic iridium films, and remain unbroken after stability testing. X-ray Photoelectron Spectroscopy confirms the iridium oxidizes during stability measurements, but retains both oxide and metallic components. (see **Figures S2-4**) Scanning Auger Electron Microscopy confirms the iridium film remains intact, with only slight carbon contamination. (**Figure S4**)

Efficiency

Finally, the n-Si/TiO_2/Ir photoanode was used in a 2-electrode format, using a wound Pt wire (surface area = 2.5 cm^2) as the counter electrode and the photocurrents, *i*, measured under 1 sun illumination as a function of applied bias, V_b (in volts), in the following electrolytes: 0.5 M H_2SO_4 (water oxidation) and (0.5 M H_2SO_4 plus 3.5 M NaCl) (chloride oxidation). These data were then used to calculate the applied bias photon-to-current efficiency (ABPE) for the photocleavage of water and the photoelectrolysis of the acidified brine by the n-Si/TiO_2/Ir photoanode under 1 sun illumination, based on the following expression:

$$\text{ABPE} = i(\text{mA cm}^{-2}) \times (E_{ref} - V_b)/P_{total}\ (\text{mW cm}^{-2}) \quad (5)$$

where, E_{ref} = 1.212 V in 0.5 M H_2SO_4 (for water oxidation) and 1.328 V in (0.5 M H_2SO_4 plus 3.5 M NaCl) (for chloride oxidation) and P_{total} = incident illumination power density = 100 mW cm^{-2}; note: this equation assumes 100% Faradaic efficiency in the production of O_2 or Cl_2.

The plots of ABPE vs V_b are illustrated in **Figure 8** and reveal maximum values for water splitting and acidified brine photoelectrolysis of 0.05 % and 1.42 %, respectively. The 28 times increase in efficiency for the photo-oxidation of the brine, compared to that of water in acid solution is primarily due to the fact that the overpotential for the former reaction is much lower than that for the latter, see **Table 1**, so that a greater fraction of the photovoltage, ca. 560 mV is utilized for fuel (H_2) and disinfectant (Cl_2) production. The ABPE value of 1.42 % compares very well with that of 0.6% reported by Kim et al.[31] for their record-breaking single crystal, worm-like hematite photoanodes for water oxidation, although, in the latter case, the value of 0.6% is flattered by the use of a 3-electrode cell, which excludes any loss in efficiency due to the counter electrode reaction, as is found for many reported ABPE and Solar to Hydrogen Efficiency (STH) values.[32] As noted earlier, ultimately the photoanode will be paired with an appropriate photocathode in a tandem cell, or be made part of a photovoltaic triple junction, which will reduce significantly the value for V_b and so improve markedly the value of ABPE. However, as it stands this is the first use of a low bandgap semiconductor photoanode to photoelectrolyze (acidified) brine so as to generate a fuel (H_2) and a disinfectant (Cl_2) with an efficiency superior to that of leading reported photoanodes used to photodissociate water.[31]

IV. Conclusion

An n-type silicon photoanode, utilizing a 2 nm thin film iridium catalyst protected by a 1.7 nm thickness coating of atomic layer deposited amorphous TiO_2, is able to effect the photo-oxidation of water to O_2 and of chloride to Cl_2, with an incident photon-to-current efficiency that increases with increasing bias voltage, eventually reaching ca. 100% efficiency if light loss due to Ir film absorption is taken into consideration. In 0.5 M H_2SO_4 acid, the photo-oxidation of water occurs at potentials that are ca. 290 mV greater than that for chloride oxidation (0.5 M H_2SO_4 plus 3.5 M NaCl), which allows the n-Si/TiO_2/Ir photoanode (1 sun illumination) and dark p+-Si/TiO_2/Ir anode to generate Cl_2 with a high (>85 %) yield. Applied bias photon-to-current efficiencies of 0.05% and 1.42 % were determined for the n-Si/TiO_2/Ir photoanode for water and chloride oxidation respectively. The latter value is particularly encouraging, especially given the potential for improvement when the n-Si/TiO_2/Ir photoanode is coupled to an appropriate photocathode in a tandem cell, or used in a triple

junction photovoltaic. This initial study illustrates the effectiveness of layered ALD-TiO_2 and Ir thin film coatings in simultaneously protecting silicon photoanodes from corrosion and achieving low overpotentials and large photovoltages to generate both a fuel but a disinfectant and a water disinfectant in a photoelectrochemical device.

References

1. Lewis, N. S. & Nocera, D. G. Powering the planet: Chemical challenges in solar energy utilization. *Proc. Natl. Acad. Sci.* **103,** 15729–15735 (2006).
2. Walter, M. G. *et al.* Solar Water Splitting Cells. *Chem. Rev. (Washington, DC, United States)* **110,** 6446–6473 (2010).
3. Rahim, S. Energy from a Water Bottle. *Scientific American* (2010). at <https://www.scientificamerican.com/article/energy-from-a-water-bottle/>
4. Reece, S. Y. *et al.* Wireless Solar Water Splitting Using Silicon-Based Semeiconductors and Earth-Abundant Catalysts. *Science (80-.).* **334,** 645–648 (2011).
5. Tilak, B. V. Kinetics of Chlorine Evolution—A Comparative Study. *J. Electrochem. Soc.* **126,** 1343 (1979).
6. EuroChlor. What is chlorine used for? (2017). at <http://www.eurochlor.org/the-chlorine-universe/what-is-chlorine-used-for.aspx>
7. Sodis. Sodis: Safe Drinking Water For All. (2016). at <http://www.sodis.ch/index_EN>
8. Beer, H. B. The Invention and Industrial Development of Metal Anodes. *J. Electrochem. Soc.* **127,** 303C (1980).
9. Hu, S. *et al.* Thin-Film Materials for the Protection of Semiconducting Photoelectrodes in Solar-Fuels Generators. *J. Phys. Chem. C* 150928141004000 (2015). doi:10.1021/acs.jpcc.5b05976
10. Aromaa, J. & Forsén, O. Evaluation of the electrochemical activity of a Ti-RuO2-TiO2 permanent anode. *Electrochim. Acta* **51,** 6104–6110 (2006).
11. Morita, M., Iwakura, C. & Tamura, H. The anodic characteristics of modified Mn oxide electrode: Ti/RuOx/MnOx. *Electrochim. Acta* **23,** 331–335 (1978).
12. Duby, P. The history of progress in dimensionally stable anodes. *JOM* **45,** 41–43

(1993).

13. Chen, Y. W. *et al.* Atomic layer-deposited tunnel oxide stabilizes silicon photoanodes for water oxidation. *Nat. Mater.* **10,** 539–544 (2011).

14. Mills, A. & Cook, A. Analysis of chlorine - oxygen gas mixtures. *Analyst* **112,** 1289–1291 (1987).

15. Meng, H., Fan, K., Low, J. & Yu, J. Electrochemically reduced graphene oxide on silicon nanowire arrays for enhanced photoelectrochemical hydrogen evolution. *Dalt. Trans.* **45,** 13717–13725 (2016).

16. Hu, S. *et al.* Amorphous TiO2 coatings stabilize Si, GaAs, and GaP photoanodes for efficient water oxidation. *Science* **344,** 1005–9 (2014).

17. Bae, D. *et al.* Back-Illuminated Si-Based Photoanode with Nickel Cobalt Oxide Catalytic Protection Layer. *ChemElectroChem* **3,** 1517 (2016).

18. Li, C. *et al.* Efficient photoelectrochemical water oxidation enabled by an amorphous metal oxide-catalyzed graphene/silicon heterojunction photoanode. *Sustain. Energy Fuels* 663–672 (2018). doi:10.1039/C7SE00504K

19. Scheuermann, A. G., Prange, J. D., Gunji, M., Chidsey, C. E. D. & McIntyre, P. C. Effects of catalyst material and atomic layer deposited TiO2 oxide thickness on the water oxidation pe rformance of metal–insulator–silicon anodes. *Energy Environ. Sci.* **6,** 2487 (2013).

20. Campet, G., Manaud, J. P., Puprichitkun, C., Sun, Z. W. & Salvador, P. Protection of photoanodes against photo-corrosion by surface deposition of oxide films: criteria for choosing the protective coating. *Act. Passiv. Electron. Components* **13,** 175–189 (1989).

21. Batzill, M., Katsiev, K., Gaspar, D. J. & Diebold, U. Variations of the local electronic surface properties of TiO2 (110) induced by intrinsic and extrinsic defects. *Phys. Rev.*

372 *B* **66,** 235401 (2002).
373 22. Papageorgiou, A. C. *et al.* Electron traps and their effect on the surface chemistry of
374 TiO2(110). *Proc. Natl. Acad. Sci.* **107,** 2391–2396 (2010).
375 23. Bagotsky, V. S. *Fundamentals of Electrochemistry*. (Wiley-Interscience, 2006).
376 24. Switzer, J. A. The n-Silicon/Thallium(III) Oxide Heterojunction Photoelectrochemical
377 Solar Cell. *J. Electrochem. Soc.* **133,** 722 (1986).
378 25. Consonni, V., Trasatti, S., Pollak, F. & O'Grady, W. E. Mechanism of chlorine
379 evolution on oxide anodes study of pH effects. *J. Electroanal. Chem.* **228,** 393–406
380 (1987).
381 26. Mozota, J. Modification of Apparent Electrocatalysis for Anodic Chlorine Evolution
382 on Electrochemically Conditioned Oxide Films at Iridium Anodes. *J. Electrochem.*
383 *Soc.* **128,** 2142 (1981).
384 27. Shinagawa, T., Garcia-Esparza, A. T. & Takanabe, K. Insight on Tafel slopes from a
385 microkinetic analysis of aqueous electrocatalysis for energy conversion. *Sci. Rep.* **5,** 1–
386 21 (2015).
387 28. McDowell, M. T. *et al.* The Influence of Structure and Processing on the Behavior of
388 TiO 2 Protective Layers for Stabilization of n-Si/TiO 2 /Ni Photoanodes for Water
389 Oxidation. *ACS Appl. Mater. Interfaces* (2015). doi:10.1021/acsami.5b00379
390 29. Hernández-Pagán, E. A. *et al.* Resistance and polarization losses in aqueous buffer-
391 membrane electrolytes for water-splitting photoelectrochemical cells. *Energy Environ.*
392 *Sci.* **5,** 7582–7589 (2012).
393 30. O'Brien, T. F., Bommaraju, T. V & Hine, F. in *Handbook of Chlor-Alkali Technology:*
394 *Volume I: Fundamentals* (Springer USA, 2005). doi:10.1007/0-306-48624-5_5
395 31. Kim, J. Y. *et al.* Single-crystalline, wormlike hematite photoanodes for efficient solar
396 water splitting. *Sci. Rep.* **3,** 1–8 (2013).

32. Chen, Z., Dinh, H. & Miller, E. *Photoelectrochemical Water Splitting: Standards, Experimental Methods, and Protocols*. (Springer, 2013).

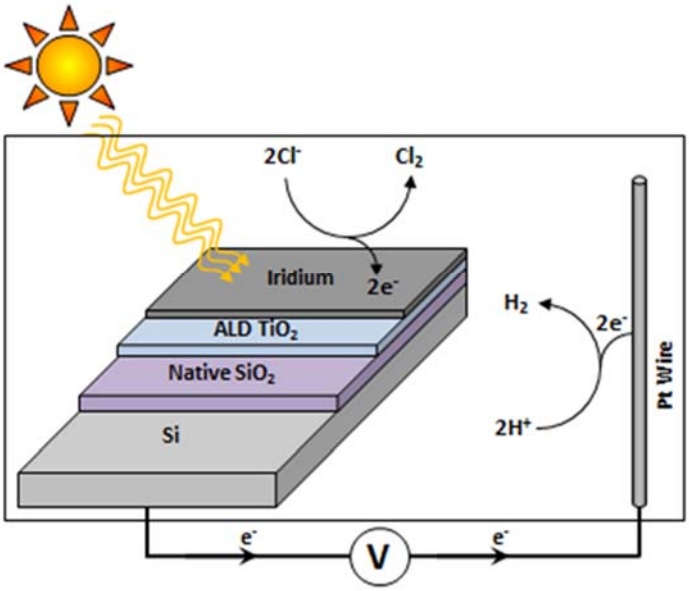

401

402 **Figure 1:** Schematic illustration of the n-Si/TiO_2/Ir photoanode used to photo-oxidize chloride (3.5 M

403 NaCl) to chlorine in acid (0.5 M H_2SO_4)

404

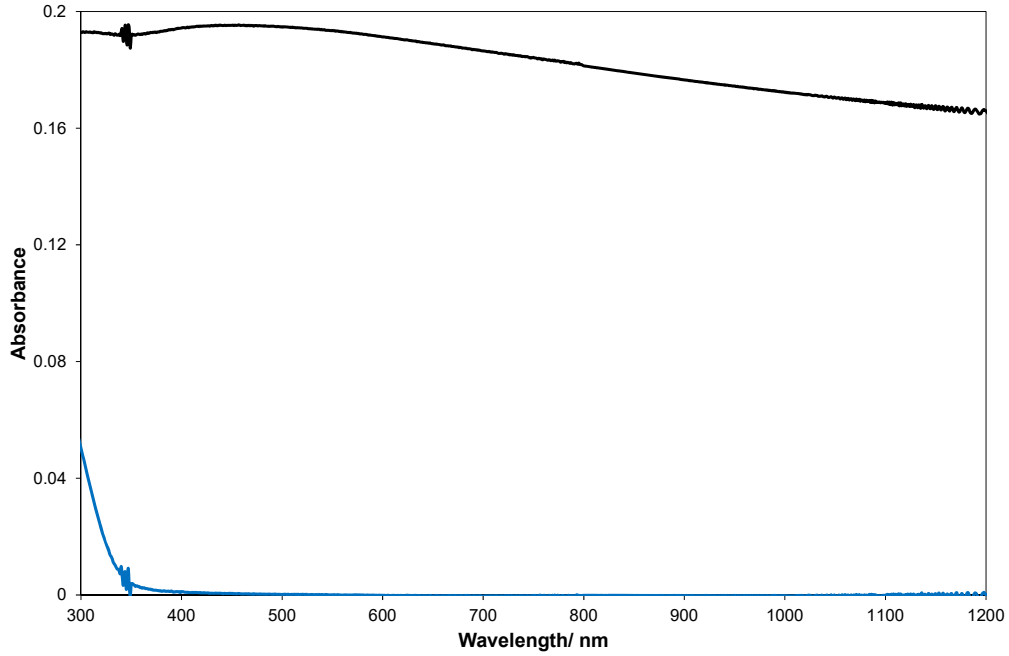

405

406 **Figure 2:** UV/Vis/NIR spectra of the following films on quartz: (i) 2 nm of evaporated Ir (black line)

407 and (ii) 1.7 nm of ALD-deposited amorphous TiO_2 (blue line).

408

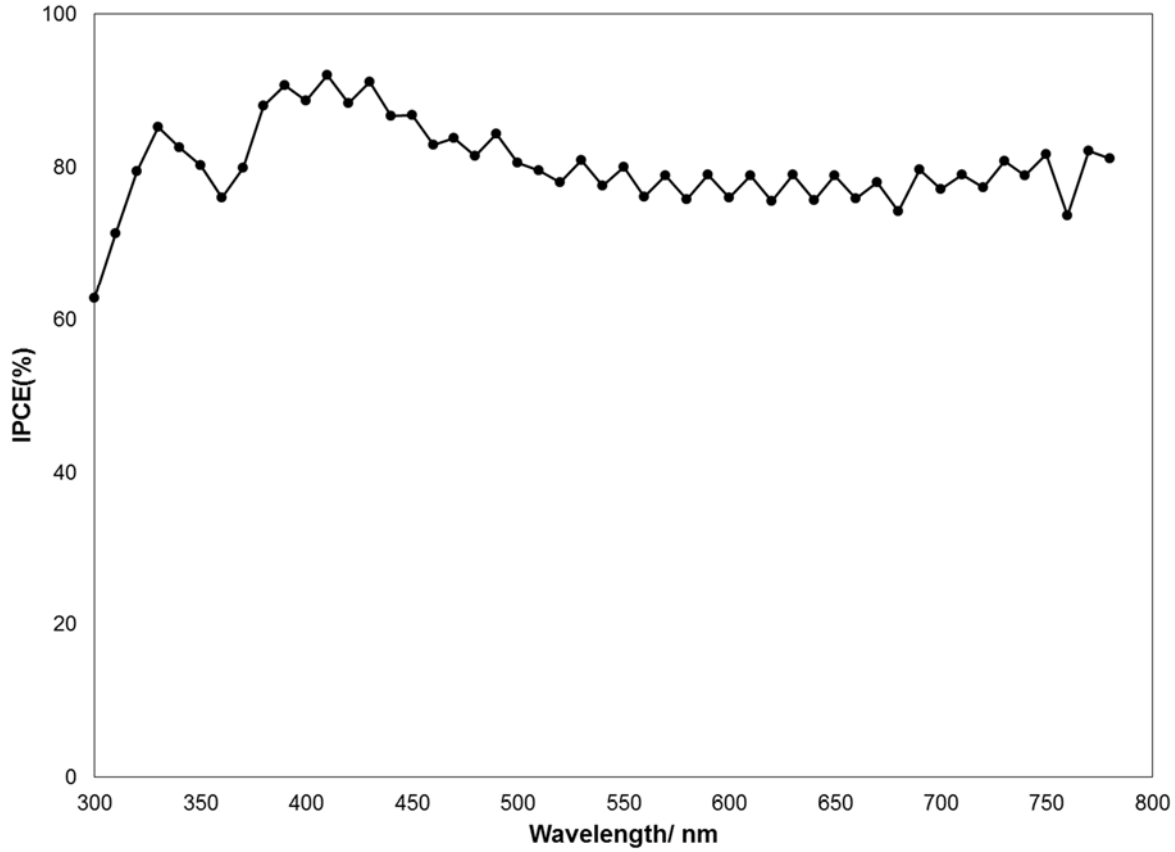

409

410 **Figure 3:** IPCE spectrum of the n-Si / 2 nm TiO_2 / 2nm Ir anode at 1.8V vs NHE and a 0.8cm^2 active

411 area. Electrolyte was 0.5 M H_2SO_4 + 3.5 M NaCl.

412

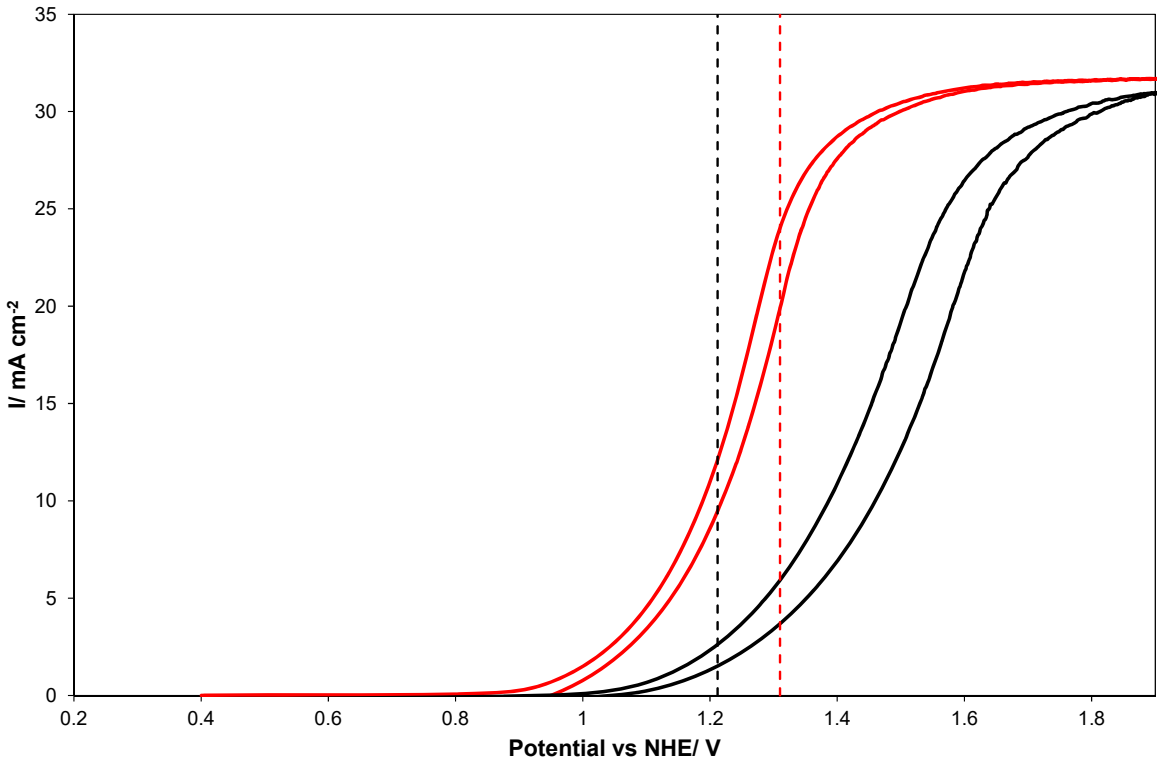

Figure 4: CVs for the n-Si/TiO_2/Ir photoanode under 1 sun irradiation, sweep rate: 100 mV s^{-1} recorded in 0.5 M H_2SO_4 (black line) or 0.5 M H_2SO_4 plus 3.5 M NaCl (red line) under 1 sun irradiation, i.e. 100 mW cm^{-2}. The broken vertical lines represent the thermodynamic potentials for reaction (1) (broken red line) ad reaction (2) (broken black line).

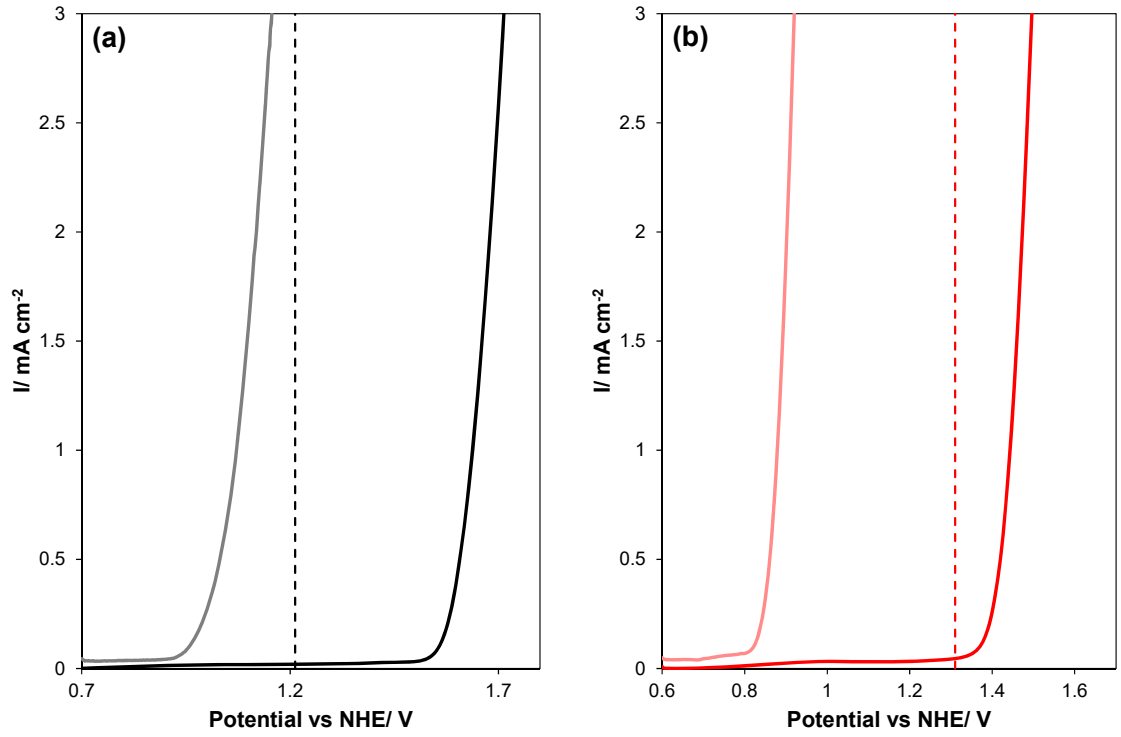

418

419 **Figure 5:** LSV curves for (from left to right): a p+-Si/TiO_2/Ir anode (in the dark) and an n-Si/TiO_2/Ir,
420 under 1 sun irradiation, in (a) 0.5 M H_2SO_4 (black lines) and (b) (0.5 M H_2SO_4 + 3.5 M NaCl), (red
421 lines) respectively. The broken vertical lines in (a) and (b) represent the thermodynamic potentials for
422 reaction (1) (red line) and reaction (2) (black line), respectively.

423 **Table 1:** Results of Tafel plot analysis of LSVs for the Si/TiO_2/Ir photoanode and p+-Si/TiO_2/Ir

424 anode

Anode	***a*/V**	***b*/V**	**V_{photo}†/V**
Water oxidation (0.5 M H_2SO_4)			
p+-Si/TiO_2/Ir	0.428 (0.332)‡	0.122	0.568 (0.532)
n-Si/TiO_2/Ir*	-0.140 (-0.200)	0.144	
Chloride oxidation (0.5 M H_2SO_4 + 3.5 M NaCl)			
p+-Si/TiO_2/Ir	0.134	0.089	0.564
n-Si/TiO_2/Ir*	-0.430	0.069	

425 * 1 sun irradiation; 1100 mW cm^{-2}

426 †: V_{photo} = photovoltage = *a*(n-Si/TiO_2/Ir*) – *a*(p+-Si/TiO_2/Ir)

427 ‡: Values reported by Chen et al in 1 M H_2SO_4

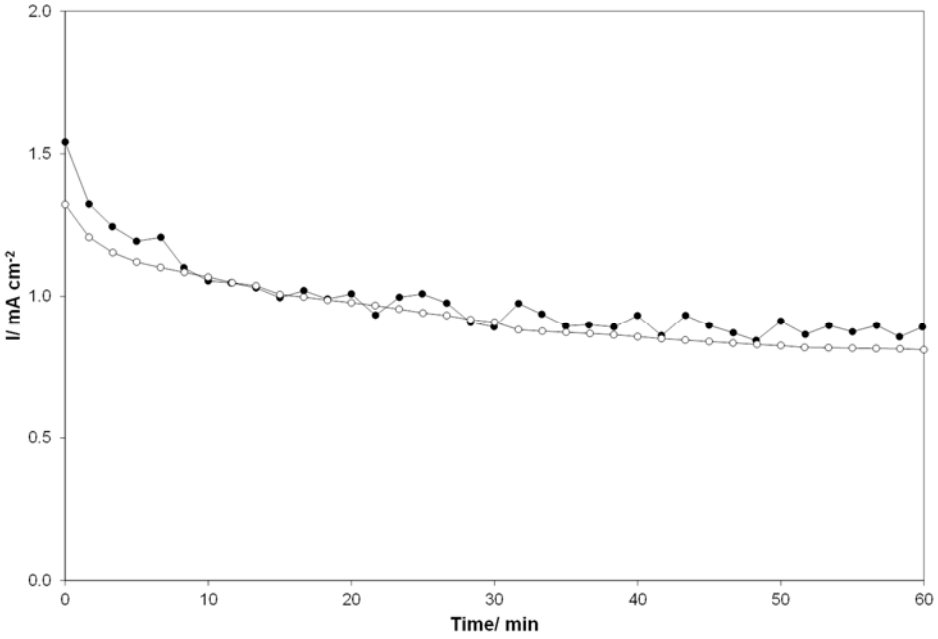

Figure 6: Chronoamperograms recorded using the electrochemical cell illustrated in figure S1 and either: (i) a Si/TiO_2/Ir photoanode, ●, (under 1 sun irradiation, polarized at 0.72 V vs Ag/AgCl), or (ii) a p+-Si/TiO_2/Ir anode, ○ (in dark, polarized at 1.18 V vs Ag/AgCl) using a electrolyte of: (0.5 M H_2SO_4 + 3.5 M NaCl).

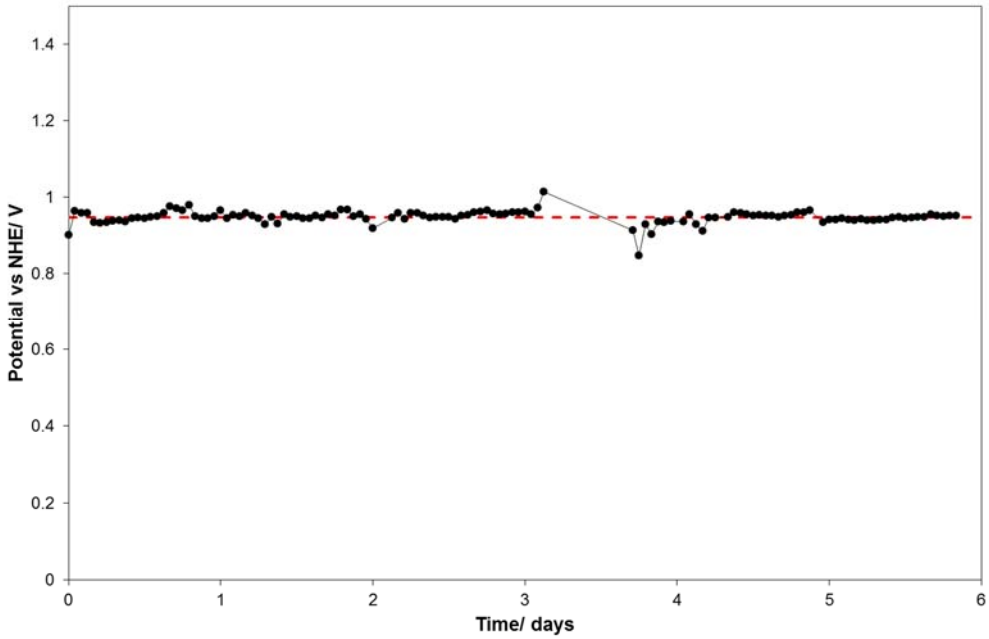

433

434 **Figure 7:** Six-day chronopotentiometry runs, at 1 mA cm^{-2}, recorded using the electrochemical cell
435 illustrated in **Figure S1** with an n-Si/TiO_2/Ir photoanode, ●, (under 455 nm LED irradiation, 6.5 mW
436 cm^{-2}), with an electrolyte of (0.5 M H_2SO_4 + 3.5 M NaCl) and the current set at 1 mA cm^{-2}. The
437 average applied potential was 0.95V (broken red line)

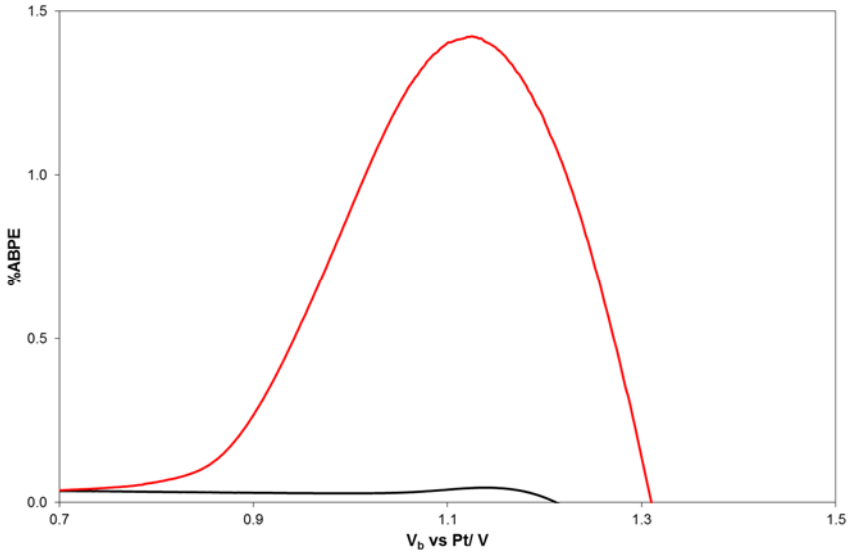

438

439 **Figure 8:** ABPE vs bias potential with respect to the Pt counter electrode, V_b plot for the n-Si/TiO_2/Ir

440 photoanode under 1 sun illumination in 0.5 M H_2SO_4 (for water oxidation – black line) and in 0.5 M

441 H_2SO_4 plus 3.5 M NaCl (for chloride oxidation – red line)